environmental microbiology

Environmental Microbiology (2018) **20**(5), 1651–1666 doi:10.1111/1462-2920.14077

Gene expression and ultrastructure of meso- and thermophilic methanotrophic consortia

Viola Krukenberg [1*†] Dietmar Riedel,[2] Harald R. Gruber-Vodicka,[1] Pier Luigi Buttigieg,[3] Halina E. Tegetmeyer,[3,4] Antje Boetius[1,3,5] and Gunter Wegener[1,5]**

[1]*Max Planck Institute for Marine Microbiology, Bremen, 28359, Germany.*

[2]*Max Planck Institute for Biophysical Chemistry, Göttingen, 37077, Germany.*

[3]*Alfred Wegener Institute, Helmholtz Center for Polar and Marine Research, Bremerhaven, 27570, Germany.*

[4]*Center for Biotechnology, Bielefeld University, Bielefeld, 33615, Germany.*

[5]*MARUM, Center for Marine Environmental Sciences, University Bremen, Bremen, 28359, Germany.*

Summary

The sulfate-dependent, anaerobic oxidation of methane (AOM) is an important sink for methane in marine environments. It is carried out between anaerobic methanotrophic archaea (ANME) and sulfate-reducing bacteria (SRB) living in syntrophic partnership. In this study, we compared the genomes, gene expression patterns and ultrastructures of three phylogenetically different microbial consortia found in hydrocarbon-rich environments under different temperature regimes: ANME-1a/HotSeep-1 (60°C), ANME-1a/Seep-SRB2 (37°C) and ANME-2c/Seep-SRB2 (20°C). All three ANME encode a reverse methanogenesis pathway: ANME-2c encodes all enzymes, while ANME-1a lacks the gene for N5,N10-methylene tetrahydromethanopterin reductase (*mer*) and encodes a methylenetetrahydrofolate reductase (Met). The bacterial partners contain the genes encoding the canonical dissimilatory sulfate reduction pathway. During AOM, all three consortia types highly expressed genes encoding for the formation of flagella or type IV pili and/or c-type cytochromes, some predicted to be extracellular. ANME-2c expressed potentially extracellular cytochromes with up to 32 hemes, whereas ANME-1a and SRB expressed less complex cytochromes ($\leq$ 8 and $\leq$ 12 heme respectively). The intercellular space of all consortia showed nanowire-like structures and heme-rich areas. These features are proposed to enable interspecies electron exchange, hence suggesting that direct electron transfer is a common mechanism to sulfate-dependent AOM, and that both partners synthesize molecules to enable it.

Received 15 November, 2017; revised 15 February, 2018; accepted 15 February, 2018. For correspondence. *E-mail vkrukenb@mpi-bremen.de, viola.krukenberg@montana.edu. Tel +494212028984, Fax +494212028870 **E-mail gwegener@mpi-bremen.de. Tel +494212028867, Fax +494212028870 †Present address: Montana State University, Bozeman, MT-59717, USA.

Introduction

In the ocean floor, the sulfate-dependent, anaerobic oxidation of methane (AOM) consumes a substantial fraction of the potent greenhouse gas methane before it can reach the hydrosphere and atmosphere (Boetius and Wenzhöfer, 2013). AOM is mediated by microbial consortia of anaerobic methanotrophic archaea (ANME) and sulfate-reducing bacteria, which couple the oxidation of methane to the reduction of sulfate via a syntrophic process (Boetius *et al.*, 2000; Orphan *et al.*, 2001b). The ANME are relatives of methanogenic archaea and use the methanogenesis pathway in reverse to oxidize methane to CO_2 (Krüger *et al.*, 2003; Hallam *et al.*, 2004; Meyerdierks *et al.*, 2005, 2010; Wang *et al.*, 2014). They are classified into at least five distinct branches of the *Methanomicrobia* (Knittel and Boetius, 2009, 2010; Haroon *et al.*, 2013), none of which contains methanogens or cultured representatives of methanotrophs. Most types of marine ANME-1 and -2 archaea form consortia with sulfate-reducing bacteria of the Seep-SRB1a or Seep-SRB2 cluster (*Desulfosarcina/Desulfococcus*; DSS; Orphan *et al.*, 2001a; Michaelis *et al.*, 2002; Knittel *et al.*, 2003; Kleindienst *et al.*, 2012; Milucka *et al.*, 2013). However, the thermophilic ANME-1 archaea associate with sulfate-reducing members of the deep-branching HotSeep-1 cluster (Holler *et al.*, 2011; Wegener *et al.*, 2015), and the psychrophilic archaea of the ANME-3 branch form consortia with bacteria of the *Desulfobulbus* cluster (Niemann *et al.*, 2006). Recent studies show that some linages of ANME-2d (including *Candidatus* Methanoperedens nitroreducens) can couple methane oxidation to the reduction of nitrate and associate

with partner bacteria that consume their toxic reaction product nitrite (Haroon *et al.*, 2013). In ANME-2/DSS consortia, Milucka and colleagues (2012) proposed that an internal cycling of zero-valent sulfur was accomplished by a partial sulfate reduction in ANME-2 and sulfur disproportionation by the partner DSS. Other types of ANME-2 were able to directly transfer reducing equivalents from methane oxidation to their partner bacteria via redox-active extracellular cytochrome c (McGlynn *et al.*, 2015). Observations of thermophilic ANME-1a/HotSeep-1 consortia suggested that this transfer was supported by nanowire-like connections presumably encoded by the *pilA* gene (Wegener *et al.*, 2015).

Here, we used enrichments of three marine AOM consortia growing at different temperature regimes [i.e., ANME-1a/HotSeep-1 (60°C), ANME-1a/Seep-SRB2 (37°C) and ANME-2c/Seep-SRB2 (20°C); Supporting Information Fig. S1] for metagenomic and -transcriptomic analyses combined with high-resolution imaging, to investigate the nature of their interaction and the molecular basis of their methane and sulfate catabolism. Recently, it was found that genomes of the ubiquitous AOM partner bacterium Seep-SRB1 encode specific, large multiheme cytochromes that may be relevant for the uptake of electrons from ANME (Skennerton *et al.*, 2017). The main focus of this study was to compare the gene expression profiles of different environmental AOM consortia, and to elucidate the key mechanisms for electron transfer and growth, including the transfer of reducing equivalents between the archaeal and bacterial partners. We tested the hypotheses that at AOM conditions a variety of ANME and SRB produce multiheme cytochromes and nanowire structures for the transfer of reducing equivalents.

Results and discussion

Microbial composition of AOM enrichments

Our AOM enrichments were retrieved by long-term ($>$ 4 years) *in vitro* cultivation at the *in situ* temperature of their corresponding sampling sites: ANME-2c/Seep-SRB2 from Elba seep sediments (20°C, E20; Ruff *et al.*, 2016), ANME-1a/Seep-SRB2 (37°C, G37) and ANME-1a/HotSeep-1 (60°C, G60) from Guaymas Basin hydrothermal sediment (Holler *et al.*, 2011; Wegener *et al.*, 2016; see Supporting Information Table S1). For Guaymas Basin samples, sediment-free enrichments were obtained after $\sim$ 2 years, while samples from Elba were sediment-free after gravimetric separation of biomass from the sand matrix (see Wegener *et al.*, 2016). Microscopic analyses showed that in these enrichments ANME and their partner bacteria grew in consortia (Fig. 1A–C, Supporting Information Fig. S1). The consortia were embedded in an extracellular polymeric matrix and contained iron sulfide precipitates as well as carbonate crystals, particularly in the G60 culture. Visible brownish-red aggregates with sizes of up to 500 μm grew in the G60 culture. Consortia sizes were considerably smaller ($<$ 100 μm, not visible by eye) in our G37 and E20 cultures. The characteristic autofluorescence of the methanogenic cofactor F_{420} was present in all ANME cells, indicative of an active methanogenesis pathway in methanogens (Doddema and Vogels, 1978) or of the reverse methanogenesis pathway in ANME (Fig. 1D–F). We noted that large coccoid ANME-1 cells ($\sim$ 2 μm diameter) dominated the G37 consortia, whereas G60 consortia contained cylindrical ANME-1 enclosed in an envelope ($\sim$ 0.7 $\times$ 1.5 μm) and the ANME-2c cells in E20 consortia formed dense sarcina-like cell packages ($\sim$ 1 μm cell diameter; Fig. 1G–I, Supporting Information Table S1). All partner bacteria could be distinguished visually from the ANME by their rod-shaped cell shape and cell diameters of $<$ 0.5 μm in E20 consortia and between 0.5 and 0.8 μm in G37 and G60 consortia (Fig. 1G–I, Supporting Information Table S1 and Supporting Information Figs. S2 and S3).

Based on the taxonomic classification of metagenomic 16S rRNA gene fragments, we inferred that the enriched community was composed of $\sim$ 33% (E20) and $\sim$ 40–56% (G37 and G60) ANME-2c and ANME-1a archaea, respectively (Fig. 1J–L, Supporting Information Fig. S4 and Supporting Information Tables S2 and S3). Similarly, we inferred that 21% (E20) to 26% (G37) of the 16S rRNA gene reads belonged to the partner bacterium Seep-SRB2; however, HotSeep-1 accounted for only 14% (G60) of the metagenomic 16S rRNA gene reads. The dominance of ANME-associated reads over those associated with their partner bacteria was even more pronounced in the proportions of 16S rRNA gene transcripts. Based on the expression of this marker gene, we associated 44% and 61–81% of all 16S rRNA gene transcripts to ANME-2c and ANME-1a, respectively. In contrast, only 10%–19% and 7% of the transcriptomic 16S rRNA gene fragments were assigned to the partner bacteria Seep-SRB2 and HotSeep-1, respectively (Fig. 1J–L, Supporting Information Fig. S4 and Supporting Information Tables S2 and S3). Together with the larger size of ANME in the consortia this suggests that they use a greater share of the energy yield from AOM under ambient conditions for growth and sustaining biomass, relative to their partner bacteria. The remaining sequences belonged to other bacteria and archaea such as *Bacteroidetes, Chloroflexi, Deferribacteres, Planctomycetes, Firmicutes, Nitrospira* or *Thaumarchaeota* (see Supporting Information Table S2).

Genomic features of ANME archaea

The reconstructed draft genomes of ANME-1b (Meyerdierks *et al.*, 2010), ANME-2d (Haroon *et al.*, 2013) and ANME-2a (Wang *et al.*, 2014) have greatly improved our understanding of these organisms' metabolic

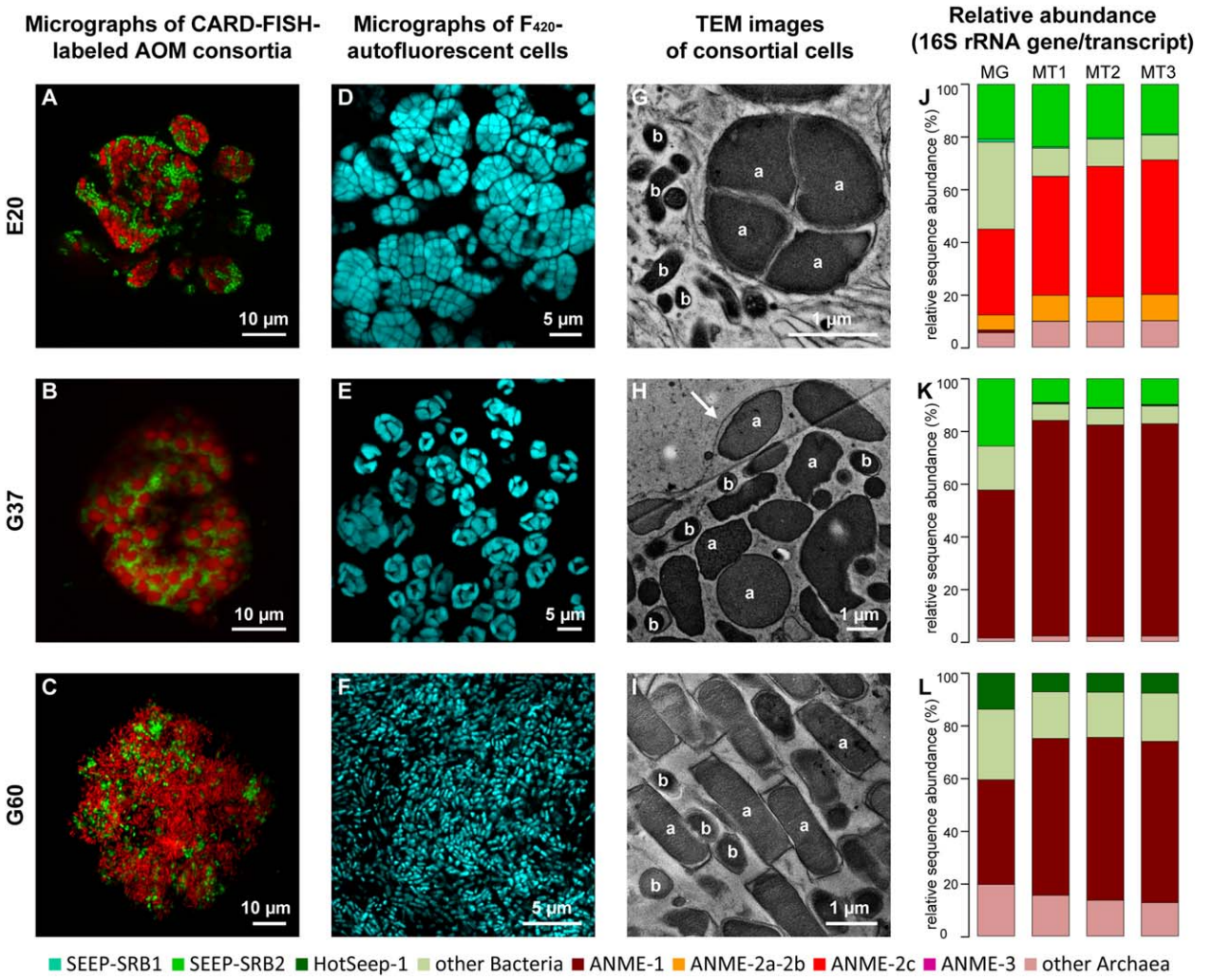

Fig. 1. Visualization and composition of long-term AOM enrichments from Elba (E20) and Guaymas Basin (G37 and G60). **A–C.** Micrographs of ANME and SRB cells labeled with CARD-FISH, present in consortia from the different enrichments: (A) ANME-2c/Seep-SRB2 from E20, (B) ANME-1a/Seep-SRB2 from G37 and (C) ANME-1a/HotSeep-1 from G60; scale bar, 10 μm. **D–F.** Autofluorescence of the methanogenic co-factor F_{420} in ANME-2c cells from E20 (D) and ANME-1 cells from G37 (E) or G60 (F); scale bar, 5 μm. **G–I**. Transmission electron micrographs showing morphology of cells within AOM consortia from E20 (G), G37 (H) and G60 (I). The 'a' and 'b' annotations indicate ANME and partner bacteria cells, respectively; while a filled arrow points to the matrix enclosing cells of a consortium (H); scale bar, 1 μm. **J–L.** Taxonomic profile of the E20 (J), G37 (K) and G60 (L) AOM enrichments based on the proportions of 16S rRNA gene and transcript fragments retrieved from metagenomes (MG) and metatranscriptomes (MT-1 to -3), respectively. See legend in Figure for color coding in J–K.

potential (see also Timmers *et al*., 2017), yet the gene expression patterns under optimal AOM conditions were not assessed. Furthermore, the substantial phylogenetic and ecological diversity within the ANME groups (Ruff *et al*., 2015) calls for greater insight into their underlying genomic variation.

Here, we retrieved a draft genome from a meso- and thermophilic ANME-1a of approximately 1.4 and 1.8 Mb (Table 1; see also Supporting Information Table S4). This size range represents about half of the assembly size previously described for psychrophilic ANME-1b (Meyerdierks *et al*., 2010). In contrast, the retrieved mesophilic ANME-2c draft genome is considerably larger with $\sim$ 3.6 Mb and similar in size to the previously described ANME-2a draft genome (Wang *et al*., 2014). Based on archaeal and euryarchaeal specific single-copy genes, the draft genomes are 96%–97% (ANME-2c, E20), 92%–94% (ANME-1a, G37) and 91%–92% (ANME-1a, G60) complete (Table 1). Notably, seven of the single-copy genes that are generally believed to be present in *Archaea* and *Euryarchaea*, were not found in the three analyzed ANME-1 data sets (the two ANME-1a from this study and ANME-1b from Meyerdierks and colleagues (2010); see Supporting Information Table S5). Further, based on single copy gene analysis the degree of contamination by other strains was $\leq$ 5% in all three draft genomes. In contrast,

Table 1. General genome properties and estimated genome completeness of the retrieved draft genomes of ANME and SRB.

	E20 ANME-2c	G37 ANME-1a	G60 ANME-1a
Size (Mb)	3.61	1.40	1.81
Scaffolds	169	5	38
GC	49	52	46
Genes	3576	1402	1877
rRNAs	5S (2), 16S, 23S	5S, 16S, 23S	5S, 16S, 23S
tRNAs	43	44	44
Missing tRNAs	Cys, Trp	Cys	Asp
Completeness[a]	96/97	94/92	92/91
Contamination[a]	5/4	2/2	4/3
Strain heterogeneity[a]	25/25	50/50	25/50
	E20 Seep-SRB2	G37 Seep-SRB2	G60 HotSeep-1
Size (Mb)	3.57	2.55	2.54
Scaffolds	166	167	1
GC	47	49	37
Genes	3334	2456	2517
rRNAs	5S, 16S, 23S	5S, 16S, 23S	5S, 16S, 23S
tRNAs	44	45	47
Missing tRNAs	His	–	–
Completeness[b]	91/94	91/95	95/96
Contamination[b]	0/1	0/1	1/2
Strain heterogeneity[b]	0/0	0/0	0/0

a. Determined with checkM (Parks *et al*., 2015) using 207 archaeal-/189 euryarchaeal-specific single copy genes.
b. Determined with checkM (Parks *et al*., 2015) using 104 bacterial-/198 deltproteobacterial-specific single copy genes.

the previously described ANME-1b dataset (Meyerdierks *et al*., 2010) from microbial mats in the Black Sea included a high strain heterogeneity and was considered to be a composite genome of several ANME-1 strains (Meyerdierks *et al*., 2010; Parks *et al*., 2015). This could account for the size discrepancy between the ANME-1b genome and the meso- and thermophilic ANME-1a genomes reported here. Notably, the genome of mesophilic ANME-1a contains a higher GC content (52%) relative to the draft genome of thermophilic ANME-1a (46%) or the low-temperature adapted ANME-1b (43%; Meyerdierks *et al*., 2010) and ANME-2c (49%), which is at odds with the view that elevated growth temperatures lead to increased GC content in ANME, as suggested in other archaea (Merkel *et al*., 2013).

ANME archaea highly express genes for reverse methanogenesis

In our experiments, we investigated ANME originating from marine enrichments, which used only methane and sulfate as redox couple to deliver energy for growth (Wegener *et al*., 2016). In the absence of sulfate or methane, neither methane oxidation nor sulfate reduction was detectable. Furthermore, ANME did not mediate methane production or showed growth when provided with other electron donors than methane over 30 days (Wegener *et al*., 2016). Hence, we attribute the detection of methanogenesis-related genes and gene transcripts in the ANME draft genomes and transcriptomes, respectively, to their role in methane oxidation. Both, ANME-1a and -2c highly express the genes necessary to produce enzymes that convert methane to CO_2 (Figs. 2 and 3, Supporting Information Tables S6 and S7). Notably, together with the 16S and 23S rRNA genes, the gene encoding the subunit A of methyl-coenzyme M reductase (*mcrA*) was among the highest expressed genes in all of the three studied ANME types, approximately 10-fold higher than the mean expression of all genes of the respective organism (Fig. 3, Supporting Information Tables S6 and S7). The McrA subunit contains the catalytic center required to activate methane, which is, due to the high activation energy required to break the C—H bond, the rate-limiting step of the overall pathway. We thus interpret the high expression of *mcr* as a means for ANME cells to sustain a large amount of Mcr protein to activate sufficient methane for cell catabolism (Krüger *et al*., 2003). Consequently, the genes encoding the enzymes that catalyze the subsequent steps of methane oxidation are less expressed (Fig. 3).

The oxidation of methane by ANME is accomplished by a strict reversal of the canonical methanogenesis pathway (ANME-2), or by introducing a modification in one step of this pathway (ANME-1). To initiate the pathway of methane oxidation, a CoM-bound methyl group is transferred to tetrahydromethanopterin (H_4MPT). Both ANME-1a draft genomes do not contain the gene encoding N5,N10-methylene tetrahydromethanopterin reductase (*mer*). The lack of the *mer* gene has also been described in genomic

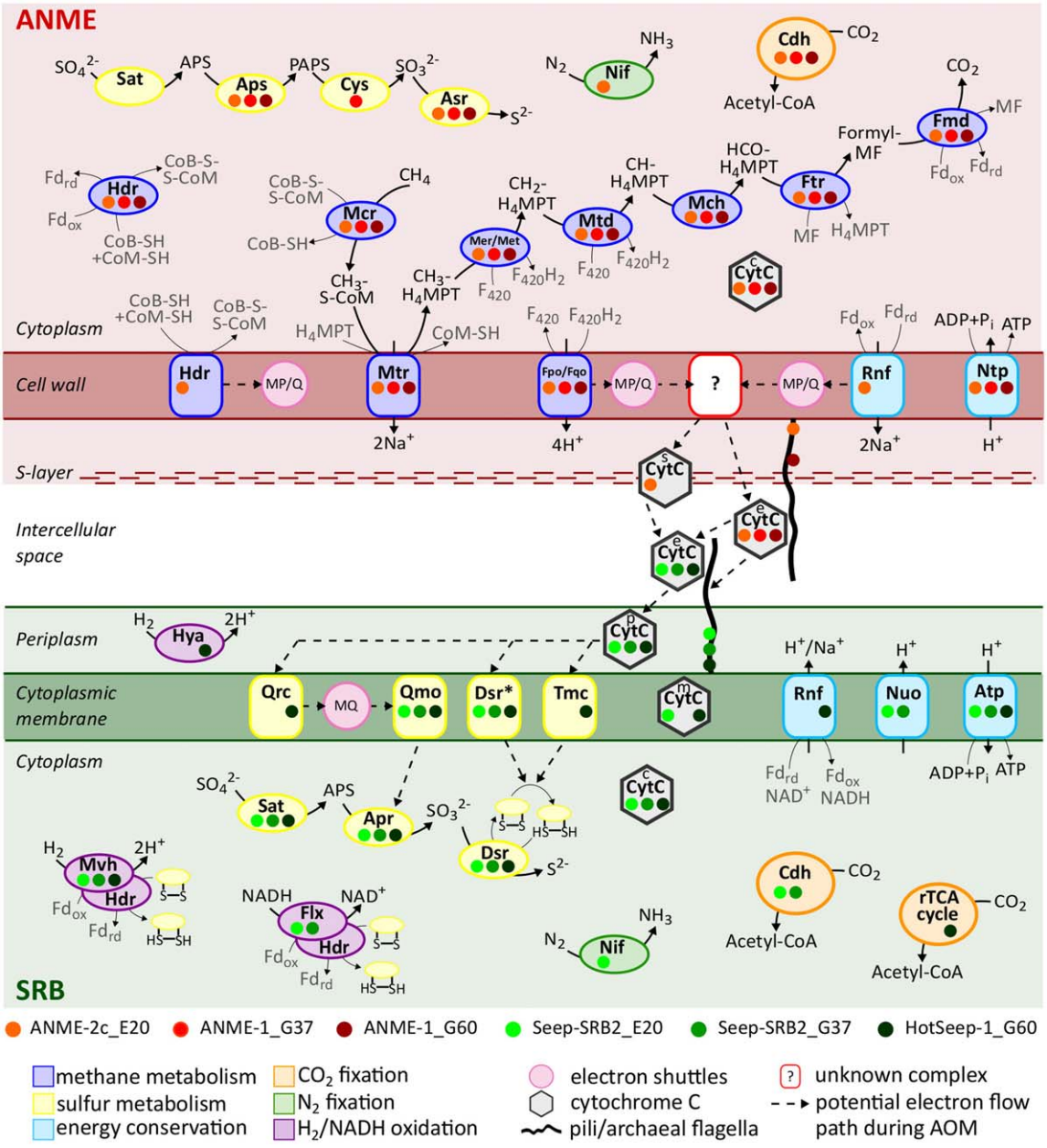

Fig. 2. Model of the metabolic capacities of the different ANME (red) and SRB (green) relevant for direct electron transfer in syntrophic AOM. Filled circles indicate the gene(s) encoding a feature are detected in the genome; circle color corresponds to clade membership (see legend in Figure); feature color indicates function, for example, methane metabolism (see legend in Figure). Predicted subcellular localization of c-type cytochromes (CytC) is indicated with lettering as follows: c, cytoplasmic; s, S-layer incorporated; e, extracellular; p, periplasmic; m, membrane-associated. Mcr, methyl-coenzyme M reductase; Mtr, tetrahydromethanopterin S-methyltransferase; Mer, 5,10-methylenetetrahydromethanopterin reductase; Met, bifunctional homocysteine S-methyltransferase/5,10-methylenetetrahydrofolate reductase; Mtd, F_{420}-dependent methylenetetrahydromethanopterin dehydrogenase; Mch, methenyltetrahydromethanopterin cyclohydrolase; Ftr, formylmethanofuran-tetrahydromethanopterin formyltransferase; Fmd, formylmethanofuran dehydrogenase; Fpo, $F_{420}H_2$:methanophenazine oxidoreductase; Fqo, $F_{420}H_2$:quinone oxidoreductase; Hdr, CoB-CoM heterodisulfide reductase; Cdh, acetyl-CoA decarbonylase/synthase complex; rTCA, reverse tricarboxylic acid cycle; Sat, sulfate adenylyltransferase; Apr, adenylylsulfate reductase; Dsr, sulfite reductase, dissimilatory-type; Qmo, quinone-interacting membrane-bound oxidoreductase complex; Dsr*, dissimilatory sulfite reductase-associated complex; Qrc, quinone reductase complex; Tmc, transmembrane complex; Aps, adenylyl-sulfate kinase; Cys, phosphoadenosine phosphosulfate reductase; Asr, sulfite reductase, assimilatory-type; Nif, nitrogenase; Rnf, electron transport complex; Nuo, NADH-quinone oxidoreductase complex; Hya, hydrogenase; Mvh/Hdr, methylviologen-reducing hydrogenase/heterodisulfide reductase complex; Flx/Hdr, flavin oxidoreductase/heterodisulfide reductase complex; Atp, ATP synthase, F-type; Ntp, ATP synthase, V-type; MP, methanophenazine; MQ, menaquinone. The F_{420}-dependent sulfite reductase detected in ANME is not shown. For further details on depicted proteins and the genomic data used in this reconstruction see Supporting Information Table S6.

data of cold-adapted ANME-1b (Meyerdierks *et al.*, 2010; Stokke *et al.*, 2012). The Mer enzyme is required for the F_{420}-dependent conversion of methyl-H_4MPT to methylene-H_4MPT and, without it, a bypass for this enzymatic step is needed. Meyerdierks and colleagues (2010) and Welander and Metcalf (2008) proposed a bypass in which the methyl group is converted to methanol and formaldehyde before re-entering the methanogenesis pathway via methylene-H_4MPT. Genes encoding a fusion protein of a formaldehyde-activating enzyme (Fae) and a hexulose-6-phosphate synthase (Hps) alongside an alcohol dehydrogenase (Adh) are present in ANME-1 to catalyze such a bypass of the Mer step. However, in both investigated ANME-1a types transcription of these genes was rather low (i.e., 0.8- to 2.2-fold higher than the geometric mean expression). While absolute expression levels cannot be quantified, such low expression levels could point to other biochemical pathways as bypass. As an alternative to the methanol bypass, Stokke and colleagues (2012) proposed a substitution of Mer by a methylenetetrahydrofolate reductase (Met). In contrast to Mer, Met is NADH-dependent and catalyzes the reduction of methylene-tetrahydrofolate (H_4F) via a two-step process in which NADH reduces FAD to $FADH_2$ and $FADH_2$ reduces methylene-H_4F to methyl-H_4F (Shima *et al.*, 2000). Both, the meso- and thermophilic ANME-1a encode the *metF* and *metV* genes (Bertsch *et al.*, 2015) and express them at levels comparable to other genes of the reverse methanogenesis pathway (Fig. 3, Supporting Information Table S6). Moreover, these genes were also present in the ANME-1b data set of Meyerdierks and colleagues (2010). Sequence comparison against the NCBI non-redundant protein database suggests that ANME-1 may have acquired their *met* genes by horizontal gene transfer from bacteria. It is, however, unclear why ANME-1 would employ this enzyme as it involves the transfer to a different cofactor. A biochemical characterization of MetFV including a metabolite analysis is required to elucidate it's functioning in methane turnover in ANME-1.

Autotrophic growth and sulfur metabolism in ANME archaea

In line with previous genomic (Meyerdierks *et al.*, 2010; Wang *et al.*, 2014) and immunolabeling (Milucka *et al.*, 2013) observations, we did not identify genes of the

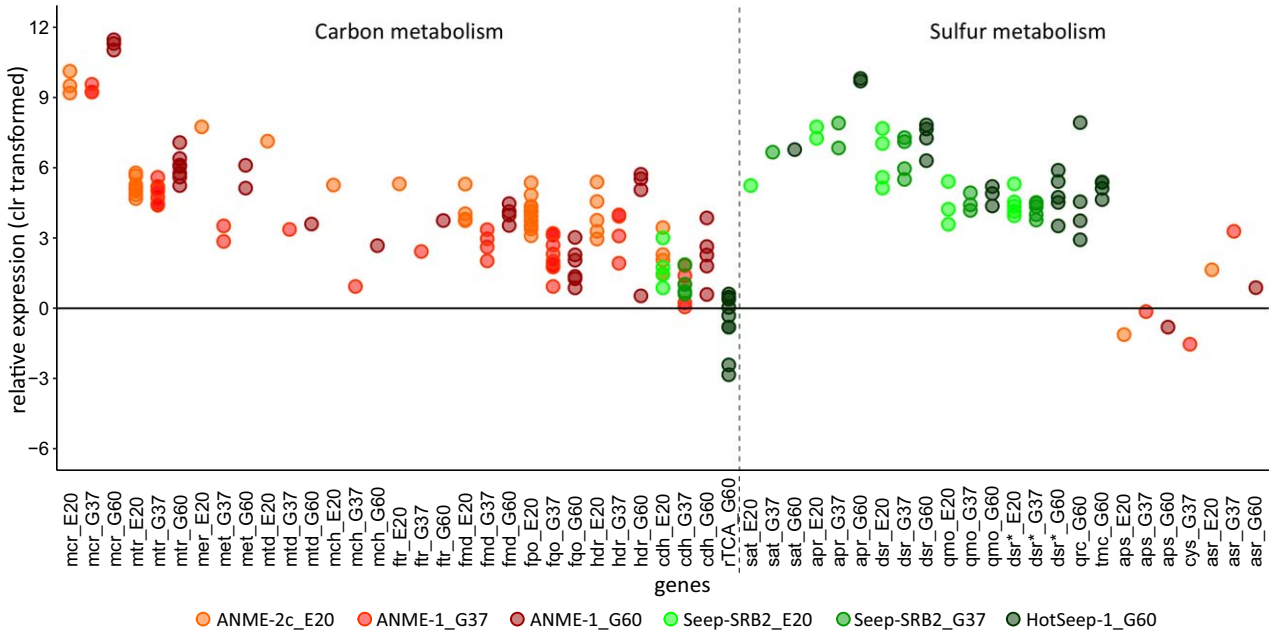

Fig. 3. Relative gene expression of ANME and SRB cells during AOM. Expression of the core enzymes of methane oxidation, sulfur metabolism and carbon fixation (colored blue, yellow or orange, respectively, in Fig. 2). Circles indicate relative median expression (n = 3 transcriptomic replicates) of a gene in a particular clade. Circle color corresponds to an ANME or SRB clade (see legend in Figure). Note, to account for different sequence counts and compositional effects in the data, the expression of a given gene is shown as a clr using a logarithm base of 2, relative to the expression of all genes of a specific clade. Zero indicates the (geometric) mean expression level, thus positive values indicate greater than mean expression while negative values indicate less than mean expression. For example, a relative expression value of 1 ($\log_2 2$) represents an expression twice as high as the geometric mean expression while a relative expression value of −1 ($\log_2 0.5$) represents an expression half that of the geometric mean expression (i.e., one-fold change in expression). For enzyme complexes, the expression of genes encoding each subunit is represented by a circle (e.g., for *mcr*, the expression of subunit A, B, C is shown by individual filled circles). If multiple copies of a gene were detected in one genome, only the most highly expressed one is shown. For gene abbreviations see legend of Fig. 2 and for details on transcriptomic data see Supporting Information Tables S6 and S7.

canonical sulfate reduction pathway in the ANME draft genomes. However, all three ANME draft genomes encode enzymes of an assimilatory sulfate reduction pathway: adenosine 5′-phosphosulfate kinase, phosphoadenosine phosphosulfate reductase and assimilatory sulfite reductase (Fig. 2). These genes showed low expression levels (Fig. 3), indicative of a function in assimilatory rather than dissimilatory sulfur metabolism. Further, the ANME-2c and ANME-1a (G37) draft genomes encode a fusion protein containing a F_{420}-reducing hydrogenase subunit B (FrhB) and a dissimilatory sulfite reductase subunit AB (DsrAB) domain. This F_{420}-dependent sulfite reductase (Fsr) has a described sulfite detoxifying function in methanogenic archaea (Johnson and Mukhopadhyay, 2005, 2008). Both ANME showed a considerable expression of this protein during AOM (i.e., 3.8- and 1.9-fold more expressed than the geometric mean expression of ANME-1 (G37) and ANME-2c, respectively, but substantially less than the *mcrA* gene; see Supporting Information Table S6). The Fsr enzyme may qualify to catalyze parts of a novel sulfate reduction pathway in ANME, as required in dissimilatory sulfur metabolism in ANME-2 (Milucka *et al*., 2012). A function of Fsr in dissimilatory sulfur metabolism has, however, not been demonstrated. Furthermore, our genomic analysis of ANME did not provide evidence for membrane-bound electron transport complexes known from sulfate reducers to link cytoplasmic sulfite reduction to energy conservation.

Based on earlier observations, the three studied ANME types produce their biomass autotrophically by the assimilation of inorganic carbon (Kellermann *et al*., 2012; Wegener *et al*., 2016). The presence of genes encoding the acetyl-CoA decarbonylase/synthase (CODH/ACS) complex in ANME is in agreement with the results of previous studies (Meyerdierks *et al*., 2005, 2010; Wang *et al*., 2014). The CODH/ACS complex combines a carbonyl and methyl group with coenzyme A (CoA) to yield acetyl-CoA, a central metabolite of the cell. These genes were expressed during AOM, confirming this route of carbon fixation in ANME (Figs. 2 and 3). In methanogens utilizing the reductive acetyl-CoA pathway, the required tetrahydromethanopterin-bound methyl group is produced in the methanogenesis pathway. Consequently, in the reversal of the methanogenesis pathway, ANME cells should be able to use a methane-derived tetrahydromethanopterin-bound methyl group for biomass generation. However, earlier experiments showed that ANME use predominantly inorganic carbon in biomass production (Kellermann *et al*., 2012; Wegener *et al*., 2016), hence they seem to use the enzymes of the methanogenesis pathway also in the reductive direction to generate CO_2-derived methyl-tetrahydromethanopterin. Employing the same enzymes for carbon fixation and energy metabolism could be beneficial for these generally energy-limited organisms, but the required mechanisms to regulate the reaction direction for the two pathways are not resolved.

As autotrophs, ANME use an inorganic nitrogen source. They express the genes for glutamate synthase and glutamine synthetase encoding a two-step conversion of ammonium to glutamate. ANME-2c additionally has genes encoding a nitrogenase (*nifDHK*; Fig. 2, Supporting Information Table S6). This supports previous reports of nitrogen fixation in ANME-2 archaea as shown in $^{15}N_2$ isotope labeling experiments (Dekas *et al*., 2009, 2015). However, the presence of genes encoding N_2-fixation is puzzling as the process is energy intensive (16 ATP per molecule of N_2 fixed), and the ANME typically inhabit very ammonium-rich and energy-limited environments. Consequently, the nitrogenase subunits of ANME-2c show only low expression during growth in the ammonium-rich medium supplied in cultivation, and it remains to be shown if nitrogen fixation occurs under ammonium limitation. The draft genomes of ANME-1a contain only the *nifH* gene, encoding one subunit of the three-membered nitrogenase, which shows sequence similarity to *nifH* genes of other ANME-1. The gene products of these subgroup IV nitrogenases are unlikely functional in nitrogen fixation (Dekas *et al*., 2015). Also, ANME-2c contains an additional isolated copy of such a *nifH* gene (Supporting Information Table S6). In ANME-2c this *nifH* gene shows an elevated expression compared to the *nifDHK* gene cluster. In contrast, in ANME-1a the *nifH* gene has only a low expression level (Supporting Information Table S6). Zheng and colleagues (2016) suggested that ANME-2d use the *nifH* gene product in the biosynthesis of cofactor F_{430}, an important element in the methyl-coenzyme M reductase. A similar functionality is likely in ANME-1a and ANME-2c, which also require large amounts of this cofactor.

Haroon and colleagues (2013) found that members of the ANME-2d clade couple methane oxidation to the reduction of nitrate to nitrite. For this ANME-2d uses a nitrate reductase encoded by *narGH*, a gene cluster that has been acquired from bacteria. Genes encoding for nitrate- or nitrite-reduction [nitrate reductase (*nar*) and nitrite reductase (*nir*)] were not present in the draft genomes of ANME-1 and -2c obtained from fully anoxic, highly sulfidic sediments.

Genomic capacities of the partner bacteria in AOM consortia

Recent studies provided insights into the draft genome of the AOM partner bacteria HotSeep-1 (Wegener *et al*., 2015; Krukenberg *et al*., 2016) and Seep-SRB1 (Skennerton *et al*., 2017). Here we analyzed the draft genome and transcriptome of two Seep-SRB2 types, representing environmentally relevant partner bacteria from a clade described by Kleindienst and colleagues (2012). The draft

genomes of the two types of Seep-SRB2 bacteria associated with the mesophilic ANME-2c and -1a had a size of 3.6 Mb (E20) and 2.6 Mb (G37), and an estimated completeness of 91%–94% and 91%–95%, respectively (see Table 1). This is in the range of what has been reported for HotSeep-1 (2.5 Mb, 97% completeness; Krukenberg *et al*., 2016) and Seep-SRB1a (~ 3 Mb; Skennerton *et al*., 2017). Congruent with our observations from the ANME draft genomes, the GC content of the partner bacteria draft genomes did not show temperature-dependent variations (47% in E20 Seep-SRB2, 49% in G37 Seep-SRB2 and 37% in G60 HotSeep-1).

As previously reported for HotSeep-1 and Seep-SRB1 (Krukenberg *et al*., 2016; Skennerton *et al*., 2017), both Seep-SRB2 draft genomes encode the core gene set for dissimilatory sulfate reduction, including membrane-bound electron transport complexes (Fig. 2), but lack genes related to methane metabolism (see Supporting Information Tables S6 and S7). Both, Seep-SRB2 and HotSeep-1 contain and express the genes for cytoplasmic sulfate reduction: sulfate adenylyltransferase (*sat*), adenosine phosphosulfate reductase (*aprAB*) and dissimilatory sulfite reductase (*dsrABCD*), as well as the membrane-bound electron transport complexes: menaquinone-interacting oxidoreductase complex (*qmoABC*) and dissimilatory sulfite reductase associated complex (*dsrMJKOP*), which are generally found to be encoded in genomes of sulfate reducers (Pereira *et al*., 2011; Rabus *et al*., 2015). The previously described draft genomes of HotSeep-1 (Krukenberg *et al*., 2016) and Seep-SRB1a (Skennerton *et al*., 2017) encode two additional membrane-bound electron transport complexes: quinone reductase complex (QrcABCD) and transmembrane complex (TmcABCD). All these membrane-bound multi-subunit complexes enable the transfer of electrons from the periplasmic cytochrome c pool to the cytoplasmic Apr and Dsr enzymes, allowing for sulfate reduction. The DsrMJKOP and TmcABCD complexes are proposed to directly transfer electrons from the periplasmic cytochrome c pool to the cytoplasmic DsrAB enyzme via the reduction of a disulfide bond in the DsrC protein (Pereira *et al*., 2011; Venceslau *et al*., 2014). In contrast, the QmoABC complex is thought to receive electrons from reduced menaquinone for the reduction of the cytoplasmic AprAB enyzme (Pires *et al*., 2003; Ramos *et al*., 2012; Grein *et al*., 2013). The QrcABCD complex is suggested to deliver electrons from periplasmic cytochromes into the membrane menaquinone pool (Venceslau *et al*., 2010), thus interacting with the Qmo complex via a menaquinone redox loop. Since we did not detect the gene set for a complete Qrc complex in the Seep-SRB2 draft genomes an alternative route for the reduction of the Qmo complex may exist in these organisms. The Qrc complex is present in most hydrogenotrophic sulfate reducers with a periplasmic hydrogenase and is proposed to be important in coupling periplasmic hydrogen oxidation to sulfate reduction (Venceslau *et al*., 2010). Our genomic data indicates that only HotSeep-1 but not Seep-SRB2 contains a periplasmic hydrogenase. Thus, HotSeep-1's Qrc complex might be primarily relevant during growth on hydrogen (see below). All three studied SRB also encode other membrane-bound and cytoplasmic complexes relevant for energy conservation. The Seep-SRB2 encode genes for the multi-subunit Nuo complex, which are present in the genomes of many sulfate reducers (Pereira *et al*., 2011). The genes for this complex were not detected in the HotSeep-1 genome. Instead, HotSeep-1 encodes the Rnf complex, which is also found in numerous sulfate reducers including Seep-SRB1, and other anaerobes (Pereira *et al*., 2011; Rabus *et al*., 2015, Skennerton *et al*., 2017). The Rnf complex is proposed to couple the exergonic reduction of NAD^+ by ferredoxin to the translocation of protons (Na^+ or H^+) across the membrane (Schmehl *et al*., 1993). This complex may also work in reverse to catalyze the reverse electron transfer from NADH to ferredoxin driven by a proton gradient (Müller *et al*., 2008). Like the Seep-SRB1 draft genome (Skennerton *et al*., 2017), both Seep-SRB2 encode the cytoplasmic Flx/Hdr complex (Ramos *et al*., 2015), which is not encoded in the HotSeep-1 draft genome. This complex couples the reduction of ferredoxin by NADH to the reduction of a disulfide bond, possibly in the DsrC protein, via electron bifurcation. During hydrogenotrophic growth of HotSeep-1 a similar reaction may be carried out by the Mvh/Hdr complex. This complex may couple hydrogen oxidation to the endergonic reduction of ferredoxin and the exergonic reduction of a heterodisulfide bond, possibly in DsrC, in a flavin-based electron bifurcation (Buckel and Thauer, 2013). Genes encoding a cytoplasmic hydrogenase (Mvh) are also contained in the Seep-SRB2 draft genomes, thus an Mvh/Hdr complex may also be present in Seep-SRB2. However, the functioning of this complex during AOM (i.e., in the absence of hydrogen as energy source) is unclear.

Like the ANME genomes, the genomes of the three partner bacteria contain the genes encoding autotrophic carbon fixation. The Seep-SRB2 genomes encode the reductive acetyl-CoA pathway, a common feature among autotrophic sulfate reducers including Seep-SRB1 (Skennerton *et al*., 2017). Notably, in the E20 and G37 enrichment, the expression of genes encoding the reductive acetyl-CoA pathway in ANME and their partner bacteria was very similar, documenting the coupled growth patterns of the two consortial members. In contrast, in the thermophile HotSeep-1, CO_2 fixation likely proceeds via the reductive tricarboxylic acid (rTCA) cycle. This alternative carbon fixation mode is often found in thermophilic microbes inhabiting hydrothermal environments (Campbell and Cary, 2004), but so far it is described for only a few sulfate reducers such as *Desulfobacter hydrogenophilus*

(Schauder *et al*., 1987; Widdel, 1987). Compared with the reductive acetyl-CoA pathway, the rTCA cycle requires approximately twice as much ATP to generate a molecule of pyruvate from CO_2. Thus, Seep-SRB1 and Seep-SRB2 might have an energetic advantage over their thermophilic counterpart HotSeep-1, but they might not be able to thrive at high temperatures.

Based on the genomic data, all three partner bacteria have the capacity to assimilate ammonium via glutamate synthase and glutamine synthetase. As described above for the ANME there is no experimental evidence for N_2 fixation in most AOM partner bacteria (Dekas *et al*., 2009; 2015). However, the Seep-SRB2 draft genome obtained from the E20 enrichment also contains a nitrogenase (*nifDHK*), suggesting at least the capacity of some Seep-SRB2 to fix molecular nitrogen. Yet the expression of the *nif* genes is very low ($\sim$ 4-fold lower than the geometric mean expression), however under cultivation conditions sufficient ammonium is always supplied.

Most AOM partner bacteria seem to be obligate syntrophs, hence they do not have the ability to grow alone. HotSeep-1, however, can grow on hydrogen as an alternative electron donor (Wegener *et al*., 2015; Krukenberg *et al*., 2016). Without an ANME partner, HotSeep-1 couples sulfate reduction to hydrogen oxidation, possibly via its periplasmic and cytoplasmic hydrogenases. Notably, also both Seep-SRB2 draft genomes encode a cytoplasmic hydrogenase (Fig. 2), whereas the Seep-SRB1 encodes a membrane-bound Ech hydrogenase (Skennerton *et al*., 2017). Hydrogenases are common features of sulfate reducers, but all previous attempts to enrich Seep-SRB2 on hydrogen were unsuccessful (Wegener *et al*., 2016), hence hydrogen is likely also not metabolized by Seep-SRB2. Although hydrogen is a well-known electron carrier in syntrophic interactions (Schink, 1997), it seems that the partner bacteria in AOM consortia never developed or completely lost the capability of hydrogen metabolism. As an exception, the thermophilic partner bacteria may have preserved hydrogen metabolism as additional trait, likely due to the generally higher probability for exposure to hydrogen in vent environments (Martin *et al*., 2008).

Interaction of ANME with their partner bacteria

We investigated the recent hypothesis that a direct exchange of reducing equivalents occurs between the members of AOM consortia (McGlynn *et al*., 2015; Wegener *et al*., 2015; Lovley, 2017). It was proposed that the transfer of electrons is mediated by large multiheme cytochromes and nanowire-like structures produced by the consortial partners (McGlynn *et al*., 2015; Wegener *et al*. 2015; Skennerton *et al*. 2017). This interaction would resemble direct electron transfer between *Geobacter* species (Summers *et al*., 2010), or consortia of *Geobacter* with different methanogens (Rotaru *et al*., 2014). In case of direct cell-to-cell contacts, extracellular c-type cytochromes might be sufficient to mediate intercellular electron transfer. Here we found that all analyzed ANME and SRB draft genomes contain the genes encoding several c-type cytochromes (Figs. 2 and 4, Table 2, Supporting Information Table S8). We categorized these cytochromes based on their predicted target localization (see 'Materials and Methods' section), and considered those with predicted extracellular, unknown or membrane-/cell wall-associated localization of potential relevance in interspecies electron transfer.

The three ANME genomes encode for two to five different cytochromes which fulfill these criteria, and for each of the organisms at least one of their cytochromes was highly expressed ($\sim$ 7-fold higher expression level than the geometric mean expression of all genes of that organism; Fig. 4A–C). McGlynn and colleagues (2015) suggested a superior role of multiheme cytochromes detected in the S-layer of ANME-2 archaea in enabling electron shuttling to their partner bacteria. Among the three here studied ANME genomes, only ANME-2c encode a c-type cytochrome in the genomic context with an S-layer-related protein. This cytochrome with 24 heme units is only moderately expressed (0.8-fold of the geometric mean expression; Fig. 4, Supporting Information Fig. S5 and Supporting Information Table S8), suggesting a minor role in electron transfer. For comparison, the highest expressed cytochrome in ANME-2c, an 8-heme cytochrome, shows an expression sevenfold greater than the geometric mean expression (Fig. 4, Supporting Information Fig. S5 and Supporting Information Table S8). Both ANME-1a archaea highly express 4-heme and 8-heme cytochromes and do not encode for cytochromes with more than 9 heme groups or for those with an S-layer domain (Fig. 4, Supporting Information Fig. S5 and Supporting Information Table S8). The latter is consistent with earlier findings for ANME-1b (McGlynn *et al*., 2015). This suggests that large S-layer associated multiheme cytochromes are not generally required for the archaeal-bacterial electron transfer.

The genomes of the bacterial consortium members encode a larger number (7 to 11) of potentially extracellular cytochromes with up to 16 heme units (Table 2, Supporting Information Table S8). However, in particular cytochromes with high heme numbers ($>$ 12) were relatively low expressed (less than 2-fold of the geometric mean; Supporting Information Fig. 5 and Supporting Information Table S8), which is substantially lower than the expression of the metabolic key gene of sulfate reduction (*dsrA*). Based on the gene expression profile of ANME and SRB, it is questionable if large multiheme cytochromes are generally involved in interspecies electron transfer. Instead, this function might be fulfilled by cytochromes with lower heme

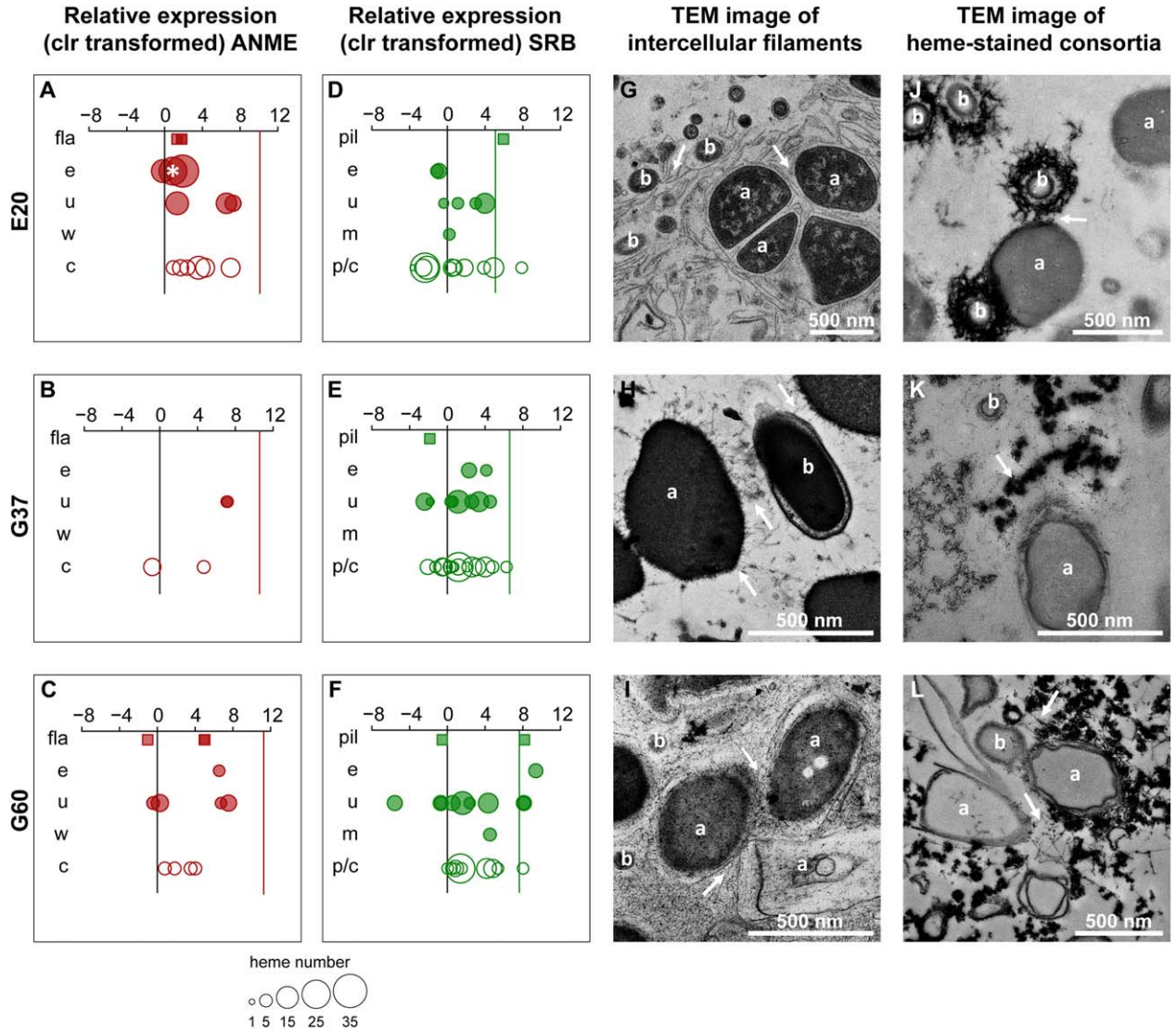

Fig. 4. Expression levels and transmission electron microscopic visualization of cytochrome c and potential extracellular structures. Expression levels in ANME (**A–C**) and expression levels in SRB (**D–F**) are shown as relative to the mean expression of all genes of the respective organism (as in Fig. 2; n = 3 transcriptomic replicates, for details see Supporting Information Tables S6 and S8). Squares indicate expression level of flagellin (*fla*) genes in ANME (red) and pilin (*pil*) genes in SRB (green). Circles indicate expression level of cytochrome c genes in ANME (red) and SRB (green). Circle size indicates number of heme units in cytochromes (based on the detection of the CXXCH motif). Cytochrome categories are based on predicted subcellular localization: e, extracellular; m, membrane (SRB only); w, cell wall (ANME only); c/p, cytoplasmic or periplasmic (SRB only); c, cytoplasmic (ANME only); u, unknown. Localization predicted using Psortb (see 'Material and Methods' section). Filled symbols indicate features with extracellular or potential extracellular localization that are potential participants in interspecies electron transfer. The white star (in row e of panel A) indicates a cytochrome c, potentially incorporated into the S-layer (detected only in ANME-2c from E20). For comparison, the median expression level of metabolic key genes for sulfate reduction (*dsrA*; green line) or methane oxidation (*mcrA*; red line) are included in A–F. **G–I.** Transmission electron microscopy (TEM) micrographs of AOM consortia showing intercellular structures. **J–L.** Transmission electron microscopy (TEM) micrographs of AOM consortia after DAB staining of heme groups to localize extracellular cytochrome c. Counterstaining was minimized in J–L, thus cell contrast is less pronounced and filaments appear less apparent than in G–I. In images G–L, 'a' indicates archaeal cells, 'b' indicates bacterial cells and filled arrows point to filaments in the intercellular space (G–I), filamentous connections between cells (G–I) and potential extracellular (J–I) or membrane associated (J,I) heme-stained cytochrome c. [Colour figure can be viewed at wileyonlinelibrary.com]

content (4-8 or 4-12 heme units in ANME and SRB, respectively; Fig. 4 and Table 2, Supporting Information Fig. S5 and Supporting Information Table S8), which are highly expressed by the three studied types of ANME and SRB.

Our genomic and transcriptomic data support the hypothesis that extracellular c-type cytochromes play an important role in archaeal-bacterial direct electron transfer. However, although cytochromes may efficiently bridge

Table 2. Overview of c-type cytochromes detected in ANME and SRB, their predicted localization and number of heme binding sites based on the CXXCH motif.

	E20		G37		G60	
Subcellular localization	ANME	SRB	ANME	SRB	ANME	SRB
Cytoplasmic or periplasmic (c/p)	6	11	2	16	4	10
Membrane- or cell wall-associated (m/w)	–	1	–	–	–	1
Extracellular (e)	3	2	–	2	1	1
Unknown (u)	3	4	2	7	4	9
Total number of c-type cytochromes	12	18	4	25	9	21

minor distances in the sub-micrometer scale, electron hopping is not possible on longer distances (Malvankar *et al*., 2012). Hence, we looked for genes encoding potential extracellular structural connections between the ANME and SRB partners. These include bacterial type IV pili, which potentially form 'nanowires' and may play a key role in microbial interspecies electron transfer (Summers *et al*., 2010; Wegener *et al*., 2015; Laso-Pérez *et al*., 2016; Lovley, 2017). Archaea can form cell appendages in form of an archaeal flagellum (i.e., archaellum), which resembles the bacterial type IV pili (Albers *et al*., 2015) and which thus might be able to also mediate electron transfer. All three genomes of the partner bacteria contain the genes required for type IV pilus assembly, including the gene encoding the major subunit, pilin (*pilA*). Notably, HotSeep-1 contains two *pilA* genes, but only one of those is highly expressed (Fig. 4). The *pilA* gene of the E20 Seep-SRB2 draft genome was likewise highly expressed whereas the expression of *pilA* by the G37 Seep-SRB2 was low (Fig. 4D–F). The ANME-1a (G60) and ANME-2c (E20) genomes encode proteins involved in the formation of archaeal flagella and the high expression of genes encoding the major subunit, flagellin, in these aggregate-bound ANME may indicate that these proteins are involved in interspecies electron transfer. However, the G37 ANME-1a genome did not contain such flagellin-encoding genes and the Seep-SRB2 partner showed only low *pilA* expression, suggesting differences between consortia types.

Using transmission electron microscopy, we examined all three AOM consortia types for extracellular structures. In all consortia it was possible to distinguish two main cell morphotypes (Fig. 1, Supporting Information Figs. S2 and S3), corresponding to ANME and bacterial cells. As previously described, the ANME-1a/HotSeep-1 consortia (G60 enrichment) form abundant filamentous structures, which connect the two partners under AOM conditions (Wegener *et al*., 2015). Examining the ANME-2c/Seep-SRB2 consortia (E20 enrichment), we also observed a network of intercellular filaments between the densely packed sarcina-like archaeal cells and the Seep-SRB2 cells. This is congruent with the high expression levels of pilin and flagellin genes in the studied organisms (Fig. 4). Consortia of the G37 enrichment contained some filamentous structures, but coherent with the low expression of *pilA* and the lack of flagellin encoding genes, these structures were far less abundant than in the other two consortia types. In the G37 consortia the archaea seem to form tight packages, possibly enclosing the partner bacteria (Fig. 1E, H). Hence in this arrangement, the proximity of the two partners may allow electron transfer by cytochromes alone.

To locate possible accumulations of cytochromes in the microbial consortia, thin sections of fixed aggregates were stained with the 3,3′-diaminobenzidine tetrahydrochloride (DAB) assay which allows detection of heme-rich regions (McGlynn *et al*., 2015). All three AOM consortia accumulated large amounts of DAB particles around archaeal and bacterial cells and in particular along intercellular filaments (Fig. 4J–L). This co-distribution of cytochrome c and filaments in the intercellular space supports an important role of these protein-derived structures in electron transfer in AOM consortia.

However, the conductivity of extracellular structures in AOM consortia potentially formed by pilin and archaeal flagellin is not yet understood. Aromatic ring structures might enable electron transfer in a conductive manner as suggested for the geopilin of *Geobacter* (Malvankar *et al*., 2011; Adhikari *et al*., 2015). Recently Walker and colleagues (2018) heterologously expressed different *pilA* genes in *Geobacter sulfurreducens* and measured the conductivity of the formed pili. In contrast to some pili produced by *G. sulfurreducens* strains with pilin encoding genes from different organisms, the one formed with the pilin from HotSeep-1 showed low conductivity (Walker *et al*., 2018); it is yet unclear if the pili of HotSeep-1 are correctly assembled by *G. sulfurreducens*. Direct conductivity measurements on pili and other extracellular structures in AOM consortia would be required to conclusively determine their electrical conductivity.

Experimental procedures

Origin and cultivation of AOM enrichments

Sediment-free AOM enrichments were established and maintained as described previously (Holler *et al*., 2011; Wegener *et al*., 2016). For a summary see Supporting Information.

Visualization of AOM consortia by fluorescence microscopy

Organisms in AOM consortia were identified using catalyzed reporter deposition fluorescence *in situ* hybridization (CARD-FISH) with clade specific probes following standard procedures (Pernthaler and Amann, 2004) and visualized with an epifluorescence or confocal laser scanning microscope (LSM 780; Zeiss; Oberkochen, Germany). The detailed employed CARD-FISH protocol can be found in the Supporting Information. Oligonucleotide probe specifications are listed in Supporting Information Table S9. To visualize the autofluorescence of cofactor F_{420}, AOM aggregates were sampled from the enrichments, transferred to microscopy slides and immediately examined using a confocal laser scanning microscope (LSM 780; Zeiss; Oberkochen, Germany) with an excitation light of 390–420 nm and a $\geq$ 463 nm emission filter.

Extraction of genomic DNA, library preparation and sequencing

For genomic DNA extraction, $\sim$ 45 ml of each AOM enrichment (E20, G37, G60) were harvested by centrifugation (5000 $\times$ g for 15 min). DNA was extracted from the pellet according to Zhou and colleagues (1996) following the protocol described by Wegener and colleagues (2016). For metagenome sequencing, 2–4 μg of high-molecular-weight DNA was used for PCR-free TruSeq paired-end and mate-pair library preparation, following the instructions of the respective Illumina library preparation kits. Paired-end libraries were prepared from $\sim$ 500 bp DNA fragments and mate-pair libraries from DNA fragments of $\sim$ 5000 bp. Libraries were sequenced on an Illumina MiSeq platform using sequencing chemistry to generate 250 bp reads.

Metagenome assembly and draft genome reconstruction

Read processing, assembly and binning procedures are described in detail in the Supporting Information. In short, raw reads were quality controlled using BBDuk (v35.14) (https://sourceforge.net/projects/bbmap/), assembled with SPAdes v3.5.0 (Bankevich *et al*., 2012) and contigs binned within the Metawatt software v3.2 (Strous *et al*., 2012). Bins of contigs identified as ANME or partner bacterium were extracted from the bulk assembly for targeted reassembly with SPAdes. Assembly quality and bin completeness was assessed using Quast (Gurevich *et al*., 2013) and CheckM (Parks *et al*., 2015). Draft genomes were automatically annotated using Prokka (Seemann, 2014) and RAST (http://rast.nmpdr.org/). Additionally, protein domains were identified by Hmmscan (Eddy, 2011) against the PfamA (database release 30; Punta *et al*., 2012) and TIGRFAM (database release 15; Haft *et al*., 2003) databases. The annotation of all genes discussed here was manually inspected and curated. To identify genes encoding cytochrome c, the draft genomes were screened for proteins with a CXXCH motif, indicative of heme-binding sites. Proteins were identified as cytochrome c if they contained at least one CXXCH motif and also matched a protein domain related to cytochrome c (see Supporting Information Table S8). The subcellular localization of potential c-type cytochromes was predicted using Psortb (Yu *et al*., 2010). Based on their predicted localization, cytochromes were assigned to the following categories: cytoplasmic or periplasmic (c/p), membrane- or cell wall-associated (m/w), extracellular (e), or, if not assigned to any of these categories, unknown (u). Note that the category 'unknown' includes also those cytochromes that had multiple alternative predictions such as e, p or m/w.

Extraction of RNA, library preparation and sequencing

Total RNA was extracted from enrichments (E20, G37, G60) incubated in triplicates under AOM conditions. The procedure for enrichment sampling, RNA preservation and extraction is detailed in the Supporting Information and follows a protocol previously described for AOM enrichments (Wegener *et al*., 2015). Total RNA was prepared for sequencing using the TruSeq stranded mRNA library prep kit (Illumina, CA) and omitting the rRNA depletion step. Synthesized cDNA was sequenced on a HiSeq instrument (HiSeq, Illumina) generating 150 bp reads.

Gene expression analysis

Quality of raw read data was assessed using FastQC and reads were processed, including adapter clipping, trimming of their 5′ and 3′ ends (5–10 bases) and removal of reads with quality $<$ 10 and length $<$ 25 bp using BBDuk (v35.14). Reads from each AOM enrichment library were mapped to the respective draft genomes with a minimum identity threshold of 98%. Reads that were unambiguously mapped to a gene were quantified with bedtools multicov (http://bedtools.readthedocs.io/en/latest/content/tools/multicov.html).

For comparative expression analysis, count data were center log ratio (clr) transformed. Prior to clr transformation a constant of 0.5 was added to all counts to prevent log(0) operations during clr transformation and counts were then standardized by gene length to account for variations. The length-standardized count data per gene in each genome were clr transformed according to the following equation:

$$\mathrm{clr_i} = \log_2\left(\frac{x_i}{\sqrt[n]{x_1 \times x_2 \times \cdots x_n}}\right)$$

with x as length-standardized counts and n as number of features per genome. Expression of selected features is presented as clr transformed values (i.e., relative to the geometric mean count of each gene per draft genome).

rRNA analysis and taxonomic classification

Quality-controlled (see above) metagenomic (paired-end forward reads) and metatranscriptomic reads were sorted using sortmeRNA (v2.1; Kopylova *et al*., 2012) into collections of reads corresponding to the bacterial 23S and 16S rRNA, the archaeal 23S and 16S rRNA, the eukaryotic 28S and 18S rRNA, the 5S rRNA and non-rRNA reads.

Reads identified as 16S rRNA (bacterial, archaeal) or 18S rRNA (eukaryotic) were taxonomically classified using the SINA aligner with the SILVA database (release SSU119; Quast *et al*., 2013). Prior to classification, data were subsampled to 3.5 Mio. reads for metatranscriptomic data and

0.1 Mio. reads for metagenomic data. Results are presented as relative abundances (%; Fig. 1) and, to account for the compositionality of the dataset, as clr transformed values (using $\log_2$; Supporting Information Fig. S4 and Supporting Information Table S3).

Heme staining and transmission electron microscopy

Heme staining was performed on AOM consortia as described by McGlynn and colleagues (2015) with some modifications, detailed in the Supplementary Information. Heme-stained AOM consortia were embedded in Agar100, thin sectioned and examined using transmission electron microscopy. Transmission electron microscopy on consortia thin sections was performed as described previously (Wegener *et al*., 2015).

Nucleotide sequence accession numbers

All sequence data are deposited in the NCBI database under the BioProject accession number PRJNA418316.

Acknowledgements

We thank Susanne Menger for culture maintenance, Mirja Meiners for laboratory assistance and Ines Kattelmann for supporting library preparation and sequencing. We also thank Andreas Teske, and the scientists of RV ATLANTIS and ALVIN team of cruise AT15–56 (2009), and Christian Lott and Miriam Weber from the Hydra Institute for Marine Sciences for providing the original vent and seep sediments. Furthermore, we greatly appreciate the bioinformatics support from Michael Richter. V.K. was funded by the DFG Leibniz program to A.B., P.L.B was supported by the European Research Council Advanced Investigator grant ABYSS 294757 to A.B., and G.W. was funded by the DFG excellence cluster MARUM, Center of Marine Environmental Sciences (Univ. Bremen). Additional funds were provided by the Max Planck Society.

References

Adhikari, R.Y., Malvankar, N.S., Tuominen, M.T., and Lovley, D.R. (2015) Conductivity of individual *Geobacter* pili. *RSC Adv* **6:** 8354–8357.

Albers, S.-V., and Jarrell, K.F. (2015) The archaellum: how Archaea swim. *Front Microbiol* **6:** 23.

Bankevich, A., Nurk, S., Antipov, D., Gurevich, A.A., Dvorkin, M., Kulikov, A.S., *et al*. (2012) SPAdes: a new genome assembly algorithm and its applications to single-cell sequencing. *J Comput Biol* **19:** 455–477.

Bertsch, J., Öppinger, C., Hess, V., Langer, J.D., and Müller, V. (2015) Heterotrimeric NADH-oxidizing methylenetetrahydrofolate reductase from the acetogenic bacterium *Acetobacterium woodii*. *J Bacteriol* **197:** 1681–1689.

Boetius, A., and Wenzhöfer, F. (2013) Seafloor oxygen consumption fuelled by methane from cold seeps. *Nat Geosci* **6:** 725–734.

Boetius, A., Ravenschlag, K., Schubert, C.J., Rickert, D., Widdel, F., Gieseke, A., *et al*. (2000) A marine microbial consortium apparently mediating anaerobic oxidation of methane. *Nature* **407:** 623–626.

Buckel, W., and Thauer, R.K. (2013) Energy conservation via electron bifurcating ferredoxin reduction and proton/Na^+ translocating ferredoxin oxidation. *Biochim Biophys Acta* **1827:** 94–113.

Campbell, B.J., and Cary, S.C. (2004) Abundance of reverse tricarboxylic acid cycle genes in free-living microorganisms at deep-sea hydrothermal vents. *Appl Environ Microbiol* **70:** 6282–6289.

Dekas, A.E., Poretsky, R.S., and Orphan, V.J. (2009) Deep-sea archaea fix and share nitrogen in methane-consuming microbial consortia. *Science* **326:** 422–426.

Dekas, A.E., Connon, S. A., Chadwick, G.L., Trembath-Reichert, E., and Orphan, V.J. (2015) Activity and interactions of methane seep microorganisms assessed by parallel transcription and FISH-NanoSIMS analyses. *ISME J* **10:** 678–692.

Doddema, H., and Vogels, G. (1978) Improved identification of methanogenic bacteria by fluorescence microscopy. *Appl Environ Microbiol* **36:** 752–754.

Dowell, F., Cardman, Z., Dasarathy, S., Kellermann, M.Y., Lipp, J.S., Ruff, S.E., *et al*. (2016) Microbial communities in methane- and short chain alkane-rich hydrothermal sediments of Guaymas Basin. *Front Microbiol* **7:** 17.

Grein, F., Ramos, A.R., Venceslau, S.S., and Pereira, I.A.C. (2013) Unifying concepts in anaerobic respiration: insights from dissimilatory sulfur metabolism. *Biochim Biophys Acta* **1827:** 145–160.

Eddy, S.R. (2011). Accelerated profile HMM searches. *PLoS Comp Biol* **7:** e1002195.

Gurevich, A., Saveliev, V., Vyahhi, N., and Tesler, G. (2013) QUAST: quality assessment tool for genome assemblies. *Bioinformatics* **29:** 1072–1075.

Hallam, S.J., Putnam, N., Preston, C.M., Detter, J.C., Rokhsar, D., Richardson, P.M., *et al*. (2004) Reverse methanogenesis: testing environmental genomics. *Science* **305:** 1457–1462.

Haft, D.H., Selengut, J.D., and White, O. (2003) The TIGRFAMs database of protein families. *Nucleic Acids Res* **31:** 371–373.

Haroon, M.F., Hu, S., Shi, Y., Imelfort, M., Keller, J., and Hugenholtz, P. (2013) Anaerobic oxidation of methane coupled to nitrate reduction in a novel archaeal lineage. *Nature* **500:** 567–570.

Holler, T., Widdel, F., Knittel, K., Amann, R., Kellermann, M.Y., Hinrichs, K.-U., *et al*. (2011) Thermophilic anaerobic oxidation of methane by marine microbial consortia. *ISME J* **5:** 1946–1956.

Johnson, E.F., and Mukhopadhyay, B. (2005) A new type of sulfite reductase, a novel coenzyme F_{420}-dependent enzyme, from the methanarchaeon *Methanocaldococcus jannaschii*. *J Biol Chem* **280:** 38776–38786.

Johnson, E.F., and Mukhopadhyay, B. (2008) Coenzyme F_{420}-dependent sulfite reductase-enabled sulfite detoxification and use of sulfite as a sole sulfur source by *Methanococcus maripaludis*. *Appl Environ Microbiol* **74:** 3591–3595.

Kellermann, M.Y., Wegener, G., Elvert, M., Yoshinaga, M.Y., Lin, Y.-S., Holler, T., *et al*. (2012) Autotrophy as a predominant mode of carbon fixation in anaerobic methane-oxidizing microbial communities. *Proc Natl Acad Sci U S A* **109:** 19321–19326.

Kleindienst, S., Ramette, A., Amann, R., and Knittel, K. (2012) Distribution and *in situ* abundance of sulfate-reducing

bacteria in diverse marine hydrocarbon seep sediments. *Environ Microbiol* **14:** 2689–2710.

Knittel, K., and Boetius, A. (2009) Anaerobic oxidation of methane: progress with an unknown process. *Annu Rev Microbiol* **63:** 311–334.

Knittel, K., and Boetius, A. (2010) Anaerobic methane oxidizers. In *Handbook of Hydrocarbon and Lipid Microbiology, Part 19 The Microbes*. Timmis, K. (ed). Berlin: Springer, pp. 2194–2202.

Knittel, K., Boetius, A., Lemke, A., Eilers, H., Lochte, K., Pfannkuche, O., *et al*. (2003) Activity, distribution, and diversity of sulfate reducers and other bacteria in sediments above gas hydrate (Cascadia Margin, Oregon). *Geomicrobiol J* **20:** 269–294.

Kopylova, E., Noé, L., Touzet, H. (2012) SortMeRNA: fast and accurate filtering of ribosomal RNAs in metatranscriptomic data. *Bioinformatics* **28:** 3211–3217.

Krüger, M., Meyerdierks, A., Glöckner, F.O., Amann, R., Widdel, F., Kube, M., *et al*. (2003) A conspicuous nickel protein in microbial mats that oxidize methane anaerobically. *Nature* **426:** 878.

Krukenberg, V., Harding, K., Richter, M., Glöckner, F.O., Gruber-Vodicka, H.R., Adam, B., *et al*. (2016) *Candidatus* Desulfofervidus auxilii, a hydrogenotrophic sulfate-reducing bacterium involved in the thermophilic anaerobic oxidation of methane. *Environ Microbiol* **18:** 3073–3091.

Laso-Pérez, R., Wegener, G., Knittel, K., Widdel, F., Harding, K.J., Krukenberg, V., *et al.* (2016) Thermophilic archaea activate butane via alkyl-CoM formation. *Nature* **539:** 1–36.

Lovley, D.R. (2017) Happy together: microbial communities that hook up to swap electrons. *ISME J* **11:** 327–310.

Malvankar, N.S., Vargas, M., Nevin, K.P., Franks, A.E., Leang, C., Kim, B.-C., *et al*. (2011) Tunable metallic-like conductivity in microbial nanowire networks. *Nat Nanotechnol* **6:** 573–579.

Malvankar, N.S., Tuominen, T., and Lovley, D.R. (2012) Lack of cytochrome involvement in long-range electron transport through conductive biofilms and nanowires of *Geobacter sulfurreducens*. *Energy Environ Sci* **5:** 8651–8659.

Martin, W., Baross, J., Kelley, D., and Russell, MJ. (2008) Hydrothermal vents and the origin of life. *Nat Rev Micro* **6:** 805–814.

McGlynn, S.E., Chadwick, G.L., Kempes, C.P., and Orphan, V.J. (2015) Single cell activity reveals direct electron transfer in methanotrophic consortia. *Nature* **526:** 531–535.

McKay, L., Klokman, V.W., Mendlovitz, H.P., LaRowe, D.E., Hoer, D.R., Albert, D., *et al*. (2016) Thermal and geochemical influences on microbial biogeography in the hydrothermal sediments of Guaymas Basin, Gulf of California. *Environ Microbiol Rep.* **8:** 150–161.

Merkel, A.Y., Huber, J.A., Chernyh, N.A., Bonch-Osmolovskaya, E.A., and Alexander, V. (2013) Detection of putatively thermophilic anaerobic methanotrophs. *Appl Environ Microbiol* **79:** 915–923.

Meyerdierks, A., Kube, M., Lombardot, T., Knittel, K., Bauer, M., Glöckner, F.O., *et al*. (2005) Insights into the genomes of archaea mediating the anaerobic oxidation of methane. *Environ Microbiol* **7:** 1937–1951.

Meyerdierks, A., Kube, M., Kostadinov, I., Teeling, H., Glöckner, F.O., Reinhardt, R., *et al*. (2010) Metagenome and mRNA expression analyses of anaerobic methanotrophic archaea of the ANME-1 group. *Environ Microbiol* **12:** 422–439.

Michaelis, W., Seifert, R., Nauhaus, K., Treude, T., Thiel, V., Blumenberg, M., *et al*. (2002) Microbial reefs in the Black Sea fueled by anaerobic oxidation of methane. *Science* **297:** 1013–1015.

Milucka, J., Ferdelman, T.G., Polerecky, L., Franzke, D., Wegener, G., Schmid, M., *et al*. (2012) Zero-valent sulphur is a key intermediate in marine methane oxidation. *Nature* **491:** 541–546.

Milucka, J., Widdel, F., and Shima, S. (2013) Immunological detection of enzymes for sulfate reduction in anaerobic methane-oxidizing consortia. *Environ Microbiol* **15:** 1561–1571.

Müller, V., Imkamp, F., Biegel, E., Schmidt, S., and Dilling, S. (2008) Discovery of a ferredoxin:NAD^+-oxidoreductase (Rnf) in *Acetobacterium woodii*: a novel potential coupling site in acetogens. *Ann NY Acad Sci* **1125:** 137–146.

Niemann, H., Lösekann, T., Beer, D.D., Elvert, M., Nadalig, T., Knittel, K., *et al*. (2006) Novel microbial communities of the Haakon Mosby mud volcano and their role as a methane sink. *Nature* **443:** 854–858.

Orphan, V.J., Hinrichs, K., Ussler, W.I., Paull, C.K., Taylor, L.T., Sylva, S.P., *et al*. (2001a) Comparative analysis of methane-oxidizing archaea and sulfate-reducing bacteria in anoxic marine sediments. *Appl Environ Microbiol* **67:** 1922–1934.

Orphan, V.J., House, C.H., Hinrichs, K.-U., McKeegan, K.D., and DeLong, E.F. (2001b) Methane-consuming archaea revealed by directly coupled isotopic and phylogenetic analysis. *Science* **293:** 484–487.

Parks, D.H., Imelfort, M., Skennerton, C.T., Hugenholtz, P., Tyson, G.W., Centre, A., *et al*. (2015) CheckM: assessing the quality of microbial genomes recoverd from isolates, single cells, and metagenomes. *Genome Res* **25:** 1043–1055.

Pereira, I.A.C., Ramos, A.R., Grein, F., Marques, M.C., da Silva, S.M., and Venceslau, S.S. (2011) A comparative genomic analysis of energy metabolism in sulfate reducing bacteria and archaea. *Front Microbiol* **2:** 69.

Pernthaler, A., and Amann, R. (2004) Simultaneous fluorescence *in situ* hybridization of mRNA and rRNA in environmental bacteria. *Appl Environ Microbiol* **70:** 5426–5433.

Pires, R.H., Lourenço, A.I., Morais, F., Teixeira, M., Xavier, A.V., Saraiva, L.M., *et al*. (2003) A novel membrane-bound respiratory complex from *Desulfovibrio desulfuricans* ATCC 27774. *Biochim Biophys Acta* **1605:** 67–82.

Punta, M., Coggill, P.C., Eberhardt, R.Y., Mistry, J., Tate, J., Boursnell, C., *et al*. (2012) The Pfam protein families database. *Nucleic Acids Res* **40**(Database issue)**:** D290–301.

Quast, C., Pruesse, E., Yilmaz, P., Gerken, J., Schweer, T., Yarza, P., *et al*. (2013) The SILVA ribosomal RNA gene database project: improved data processing and web-based tools. *Nucleic Acids Res* **41**(Database issue)**:** D590–596.

Rabus, R., Venceslau, S.S., Wöhlbrand, L., Voordouw, G., Wall, J.D., and Pereira, I.A. (2015) A post-genomic view of the ecophysiology, catabolism and biotechnological relevance of sulphate-reducing prokaryotes. *Adv Microb Physiol* **66:** 55–321.

Ramos, A.R., Keller, K.L., Wall, J.D., and Pereira, I.A.C. (2012) The membrane QmoABC complex interacts directly

with the dissimilatory adenosine 5'-phosphosulfate reductase in sulfate reducing bacteria. *Front Microbiol* **3:** 137.
Ramos, A.R., Grein, F., Oliveira, G.P., Venceslau, S.S., Keller, K.L., Wall, J.D., *et al.* (2015) The FlxABCD-HdrABC proteins correspond to a novel NADH dehydrogenase/heterodisulfide reductase widespread in anaerobic bacteria and involved in ethanol metabolism in *Desulfovibrio vulgaris* Hildenborough. *Environ Microbiol* **17:** 2288–2305.
Rotaru, A.-E., Shrestha, P.M., Liu, F., Shrestha, M., Shrestha, D., Embree, M., *et al.* (2014) A new model for electron flow during anaerobic digestion: direct interspecies electron transfer to *Methanosaeta* for the reduction of carbon dioxide to methane. *Energy Environ Sci* **7:** 408.
Ruff, S.E., Kuhfuss, H., Wegener, G., Lott, C., Ramette, A., Wiedling, J., *et al.* (2016) Methane seep in shallow-water permeable sediment harbors high diversity of anaerobic methanotrophic communities, Elba, Italy. *Front Microbiol* **7:** 1–20.
Schauder, R., Widdel, F., and Fuchs, G. (1987) Carbon assimilation pathways in sulfate-reducing bacteria II. Enzymes of a reductive citric acid cycle in the autotrophic *Desulfobacter hydrgenophilus*. *Arch Microbiol* **148:** 218–225.
Schink, B. (1997) Energetics of syntrophic cooperation in methanogenic degradation. *Microbiol Mol Biol Rev* **61:** 262–280.
Schmehl, M., Jahn, A., Meyer zu Vilsendorf, A., Hennecke, S., Masepohl, B., Schuppler, M., *et al.* (1993) Identification of a new class of nitrogen fixation genes in *Rhodobacter capsulatus*: a putative membrane complex involved in electron transport to nitrogenase. *Mol Gen Genet* **241:** 602–615.
Seemann, T. (2014) Prokka: rapid prokaryotic genome annotation. *Bioinformatics* **30:** 2068–2069.
Shima, S., Warkentin, E., Grabarse, W., Sordel, M., Wicke, M., Thauer, R.K., *et al.* (2000) Structure of coenzyme F_{420}-dependent methylenetetrahydromethanopterin reductase from two methanogenic Archaea. *J Mol Biol* **300:** 935–950.
Skennerton, C.T., Chourey, K., Iyer, R., Hettich, R.L., Tyson, G.W., and Orphan, V.J. (2017) Methane-fueled syntrophy through extracellular electron transfer: uncovering the genomic traits conserved within diverse bacterial partners of anaerobic methanotrophic archaea. *MBio* **8:** e00530–e00517.
Stokke, R., Roalkvam, I., Lanzen, A., Haflidason, H., and Steen, I.H. (2012) Integrated metagenomic and metaproteomic analyses of an ANME-1-dominated community in marine cold seep sediments. *Environ Microbiol* **14:** 1333–1346.
Strous, M., Kraft, B., Bisdorf, R., and Tegetmeyer, H.E. (2012) The binning of metagenomic contigs for microbial physiology of mixed cultures. *Font Microbiol* **3:** 1–11.
Summers, Z.M., Fogarty, H.E., Leang, C., Franks, A.E., Malvankar, N.S., and Lovley, D.R. (2010) Direct exchange of electrons within aggregates of an evolved syntrophic coculture of anaerobic bacteria. *Science* **330:** 1413–1415.
Timmers, P.H.A., Welte, C.U., Koehorst, J.J., Plugge, C.M., Jetten, M.S.M., and Stams, A.J.M. (2017) Reverse methanogenesis and respiration in methanotrophic archaea. *Archaea* **2017:** 1654237.
Venceslau, S.S., Lino, R.R., and Pereira, I.A.C. (2010) The Qrc membrane complex, related to the alternative complex III, is a menaquinone reductase involved in sulfate respiration. *J Biol Chem* **285:** 22774–22783.
Venceslau, S.S., Stockdreher, Y., Dahl, C., and Pereira, I.A.C. (2014) The 'bacterial heterodisulfide' DsrC is a key protein in dissimilatory sulfur metabolism. *Biochim Biophys Acta* **1837:** 1148–1164.
Walker, D.J.F., Ramesh, Y., Adhikari, R.Y., Holmes, D.E., Ward, J.E., Woodard, T.L., *et al.* (2018) Electrically conductive pili from pilin genes of phylogenetically diverse microorganisms. *ISME J* **12:** 48–58.
Wang, F., Zhang, Y., Chen, Y., He, Y., Qi, J., Hinrichs, K., *et al.* (2014) Methanotrophic archaea possessing diverging pathways. *ISME J* **8:** 1069–1078.
Wegener, G., Krukenberg, V., Riedel, D., Tegetmeyer, H.E., and Boetius, A. (2015) Intercellular wiring enables electron transfer between methanotrophic archaea and bacteria. *Nature* **526:** 587–590.
Wegener, G., Krukenberg, V., Ruff, S.E., Kellermann, M.Y., and Knittel, K. (2016) Metabolic capabilities of microorganisms involved in and associated with the anaerobic oxidation of methane. *Front Microbiol* **7:** 1–16.
Welander, P.V., and Metcalf, W.W. (2008) Mutagenesis of the C1 oxidation pathway in *Methanosarcina barkeri*: new insights into the Mtr/Mer bypass pathway. *J Bacteriol* **190:** 1928–1936.
Widdel, F. (1987) New types of acetate-oxidizing, sulfate-reducing *Desulfobacter* species, *D. hydrogenophilus* sp. nov., *D. latus* sp. nov., and *D. curvatus* sp. nov. *Arch Microbiol* **148:** 286–291.
Yu, N.Y., Wagner, J.R., Laird, M.R., Melli, G., Rey, S., Lo, R., *et al.* (2010) PSORTb 3.0: improved protein subcellular localization prediction with refined localization subcategories and predictive capabilities for all prokaryotes. *Bioinformatics* **26:** 1608–1615.
Zheng, K., Ngo, P.D., Owens, V.L., and Yang, X. (2016) The biosynthetic pathway of coenzyme F_{430} in methanogenic and methanotrophic archaea. *Science* **354:** 339–342.
Zhou, J., Bruns, M.A.N.N., Tiedje, J.M. (1996) DNA recovery from soils of diverse composition. *Appl Environ Microbiol* **62:** 316–322.

Supporting information

Additional supporting information may be found in the online version of this article at the publisher's website.

Fig. S1. Phylogenetic affiliation of ANME and partner bacteria clades within *Methanomicrobia* and *Deltaproteobacteria*. In the E20 enrichment ANME-2c forms consortia with Seep-SRB2, in the G37 enrichment ANME-1 forms consortia with Seep-SRB2, and in the G60 enrichment ANME-1 forms consortia with HotSeep-1. The phylogenetic trees are modified from Wegener and colleagues (2016). Phylogeny was inferred with RAxML based on 16S rRNA gene variation; ANME clades are shown in red, partner bacteria clades are shown in green; grey dashed lines connect the dominant partner organisms detected in the consortia. Note that the phylogenetic affiliation of HotSeep-1 based on the 16S rRNA gene is currently not well resolved and its placement within the *Deltaproteobacteria* is debatable (see Dowell *et al.*, 2016; McKay *et al.*, 2016; Krukenberg *et al.*, 2016).
Fig. S2. Transmission electron microscopy images of AOM consortia thin sections from the E20 enrichment. (A) archaeal cells; (B) bacterial cells; arrows point to areas of

interest (i.e., cell appendages and filaments in the intercellular space).

Fig. S3. Transmission electron microscopy images of AOM consortia thin sections from the G37 enrichment. (A) archaeal cells; (B) bacterial cells; arrows point to areas of interest (i.e., cell appendages and filaments in the intercellular space).

Fig. S4. Relative abundance of 16S rRNA gene and transcript fragments in AOM enrichments E20, G37 and G60. To account for different sequence counts and compositional effects in the data, the relative abundance of a given clade is shown as a clr using a logarithm base of 2. Zero indicates the (geometric) mean abundance level of clades in a given sample, thus positive values indicate greater than the mean abundance while negative values indicate less than the mean abundance. MG, metagenomic; MT, metatranscriptomic (3 replicates).

Fig. S5. Relation between heme content and relative expression of c-type cytochromes in ANME and SRB from AOM enrichments E20, G37, G60. The expression is shown as a clr using a logarithm base of 2, relative to the expression of all genes of a specific clade. The line at zero indicates the (geometric) mean expression level, thus positive values indicate greater than mean expression while negative values indicate less than mean expression. Red circles: c-type cytochromes of ANME; green circles: c-type cytochromes of SRB.

Table S1. Characteristics of the AOM consortia enrichments studied in this work.

Table S2. Classification of metagenomic and metatranscriptomic 16S rRNA gene fragments on different phylogenetic levels.

Table S3. Summary of 16S rRNA gene fragments obtained from enrichments E20, G37 and G60 presented as read count data and compositionality corrected data.

Table S4. Comparison of 16S rRNA and metabolic marker genes of ANME and SRB.

Table S5. Single copy genes identified in ANME draft genomes.

Table S6. Overview of gene expression data of ANME and SRB.

Table S7. Draft genomes and expression data generated in this study.

Table S8. Overview of c-type cytochromes encoded in the ANME and SRB draft genomes.

Table S9. Overview of clade specific oligonucleotide probes used in CARD-FISH experiments in this study.